



Design and fabrication of photonic devices and a microfluidic channel with a femtosecond laser

Diseño y fabricación de dispositivos fotónicos y un canal microfluídico con láser de femtosegundos

Jiménez-Ávila Daniel

Instituto Tecnológico de Aguascalientes
Departamento de Ingeniería Electrónica
Centro de Investigaciones en Óptica, A. C.
Laboratorio de Óptica Integrada
E-mail: R15150530@aguascalientes.tecnm.mx
<https://orcid.org/0000-0002-8719-8907>

Vázquez Gloria V.

Centro de Investigaciones en Óptica, A. C.
Laboratorio de Óptica Integrada
E-mail: gvazquez@cio.mx
<https://orcid.org/0000-0002-9593-5524>

Soto-Bernal Juan José

Instituto Tecnológico de Aguascalientes
Departamento de Ingeniería Electrónica
E-mail: juan.sb@aguascalientes.tecnm.mx
<https://orcid.org/0000-0001-6316-2160>

Abstract

This article presents the modeling and fabrication of photonic devices such as a Mach-Zehnder waveguide interferometer (MZWI) and a 1×4 optical power splitter (OPS) with a microfluidic channel. The photonic structures were designed using CAD software and BeamPROP™ to have an s-shaped waveguide bend geometry and a total length of $8000 \mu\text{m}$, and the devices were then integrated with a $6000 \mu\text{m}$ microfluidic channel to form configurations based on conical spirals and helices with femtosecond laser radiation. The entire writing process was performed in a single step with a 20X microscope objective to achieve greater accuracy in the manufacturing process. A chemical etching step was performed using the shape-controlled with femtosecond laser irradiation followed by chemical etching (SC-FLICE) technique, forming a uniform cross-section in the central part of the microfluidic channel. The energy doses and translation speeds of the system were varied, resulting in a longer microfluidic channel. In this research, we introduce an optofluidic system which integrates the principles of optics and microfluidics, is suitable for biosensing applications. The compatibility of this system with biosensing applications paves the way for significant progress in various sectors, including medical diagnostics, environmental surveillance, and biochemical studies. The originality and value of this work lie in its unique design and potential for broad application. In the present work, it was demonstrated that using ultrafast laser writing, we can fabricate photonic devices and a consistent microfluidic channel on a single step.

Keywords: Photonic devices, integrated optics, BeamPROP™, microfluidic channel, femtosecond laser, chemical etching, micromachining.

Resumen

Este artículo presenta el modelado y fabricación de dispositivos fotónicos como el interferómetro de guías de onda Mach-Zehnder (MZWI, por sus siglas en inglés) y un divisor de potencia óptica de guías de onda (OPS, por sus siglas en inglés) de 1×4 con un canal microfluídico. Las estructuras fotónicas se diseñaron utilizando software CAD y BeamPROP™ para tener una geometría de curvatura de guía de onda en forma de "s" y una longitud total de $8000 \mu\text{m}$, luego los dispositivos se integraron con un canal microfluídico de $6000 \mu\text{m}$ para formar configuraciones basadas en espirales y hélices cónicas mediante radiación láser de femtosegundos. Todo el proceso de escritura se realizó en un solo paso con un objetivo de microscopio de 20X para lograr una mayor precisión en el proceso de fabricación. Se realizó un paso de grabado químico utilizando la técnica de forma controlada mediante irradiación con láser de femtosegundos seguido de grabado químico (SC-FLICE, por sus siglas en inglés), formando una sección transversal uniforme en la parte central del canal microfluídico. Se variaron las dosis de energía y las velocidades de traslación del sistema, lo que resultó en un canal microfluídico más largo. En esta investigación, presentamos un sistema optofluídico que integra los principios de la óptica y la microfluídica que es adecuado para aplicaciones de biodetección. La compatibilidad de este sistema con aplicaciones de biosensores allana el camino para avances significativos en diversos sectores, incluidos el diagnóstico médico, la vigilancia ambiental y los estudios bioquímicos. La originalidad y el valor de este trabajo residen en su diseño único y su potencial para una amplia aplicación. En el presente trabajo se demostró que, utilizando la escritura láser ultrarrápida, podemos fabricar dispositivos fotónicos y un canal microfluídico consistente en un solo paso.

Descriptores: Dispositivos fotónicos, óptica integrada, BeamPROP™, canal microfluídico, láser de femtosegundos, grabado químico, micromaquinado.

INTRODUCTION

In recent years, optofluidic systems have been developed within a single substrate by combining optical techniques with fluidic methods, resulting in an enormous diversity of features that are useful for many applications (Chandrahilim *et al.*, 2015). Consequently, in the ongoing search for improved reduced systems for chemical and biological analysis, lab-on-a-chip devices (LOCs) have been manufactured. These devices are compact, efficient, and provide more free space in work areas because they allow more studies to be carried out in record times while providing an excellent response and capacity at a low cost (Haque *et al.*, 2014). These devices require a set of microfluidic channels to transport, mix, separate, and analyze various samples with volumes in the order of microliters to nanoliters. Some of the advantages of LOCs include increased sensitivity and analysis speed, standardized and automated measurement parameters, and reduced consumption of samples and laboratory reagents (Osellame *et al.*, 2011). On the other hand, optical waveguides allow the manufacture of flexible structures such as multiplexers and splitters in straight and curved shapes (Kee *et al.*, 2008). Thus, different configurations of integrated photonic devices for sensing, such as microring resonators (Luchansky & Bailey, 2012), surface plasmon resonators (Bing *et al.*, 2012), long-period gratings (Pham *et al.*, 2012), Mach-Zehnder interferometers (Xia *et al.*, 2012; Yadav *et al.*, 2014), and power splitters (Liu *et al.*, 2017a), have been reported. In particular, the MZWI is effective for real-time monitoring, and its detection principle is achieved by means of waveguides that form two Y-shaped branches, which are defined as a reference branch and a measurement branch (sensing window). By passing a beam of light through each branch, the light speed (phase) changes, and because of optical interference, the intensity of the light changes at the exit of the waveguide (Patel & Hamde, 2017). Therefore, functionalizing one of these optical path lengths locally changes the refractive index and induces a shift in the transmission spectrum (Heideman & Lambeck, 1999). In addition, OPS are optimally compact structures that divide the input power into equal parts without significant reflection losses (Olyaei *et al.*, 2020). In most cases, they require bent waveguides to interconnect routes with other devices using the back-to-back waveguide bend geometry (Devayani *et al.*, 2014). Thus, an array of photodiodes (detectors) can easily detect changes in light intensity owing to the presence of a biological/chemical substance (Leistikko & Jensen, 1998). Currently, new applications of integrated photonics are being developed, owing to the 3D union of optical elements

with microfluidic channels, which has optimized optofluidic systems and increased their detection efficiency (Haque *et al.*, 2014). One of the most commonly used materials for sensing processes in microfluidic systems is fused silica glass (Zhao *et al.*, 2015), which has good chemical consistency, extensive spectral transmission, and low fluorescence (Zhao *et al.*, 2015; Rajesh & Bellouard, 2010). Fused silica has been used as a vitreous material in the manufacture of 3D microsystems by means of the FLICE technique (Liu *et al.*, 2014). In this method, a three-dimensional structure is irradiated with a femtosecond laser focused on the substrate (where a femtosecond (fs) is equal to 10^{-15} seconds); subsequently, the modified area is etched with an aqueous solution of hydrofluoric acid (HF) (Paiè *et al.*, 2016). Another method for obtaining microfluidic channels with a uniform cylindrical shape is the SC-FLICE method, which is based on etching a cone opposite to that achieved with the FLICE technique to compensate for its initial conical shape (Vishnubhatla *et al.*, 2009). In addition, this method includes attributes such as the ability to handle three-dimensional structures, superior flexibility, and optical and fluidic elements with high accuracy (greater than 100 nm) (Bellini *et al.*, 2012). Therefore, the ability to integrate microfluidic arrays and optical waveguides into the same device has enabled the development of novel optofluidic systems (Asrar *et al.*, 2015; Gao *et al.*, 2016; Martinez-Vazquez *et al.*, 2015) for the manipulation and analysis of individual particles with high precision (Paiè *et al.*, 2014). Various applications of such platforms have been reported, such as in cytology at the single-cell level, in which the study of a specific cell allows observation of the changes from one cell to another in a predetermined set, in the measurement of rhodamine concentration (Li *et al.*, 2015), and in the detection of heavy metals in aqueous media, such as mercury (Hg^{2+}), which has a high degree of toxicity in the body and the environment and can cause serious health problems (Liu *et al.*, 2017b). The present work focuses on the modeling, design, simulation, fabrication, and characterization of two photonic device configurations, a MZWI and a 1×4 OPS with an s-shaped waveguide bend geometry; the structures have a total length of 8000 μm and were developed in AutoCAD[®] and simulated in BeamPROP[™]. These devices were integrated with a 6000 μm microfluidic channel with configurations based on conical spirals and helices with femtosecond laser writing, and the entire writing process was completed in one step with a 20X microscope objective to improve precision in the manufacturing process. Subsequently, the SC-FLICE technique was used for chemical etching, resulting in a uniform cross-section at the center of the microfluidic channel. These

integrated structures have been proposed for the development of an optical biosensor.

MODELING OF PHOTONIC DEVICES

MZWI

In a standard MZWI structure, as a result of the combination of the interference areas in each of its branches, there is a phase difference $\Delta\varphi_m$ (the magnitude of which is measured) between both beams. Consequently, the phase shift $\Delta\varphi_m$ is a function of the difference in effective refractive index of the measuring area and the length of the measurement branch (Heideman & Lambeck, 1999), which is given by equation (1):

$$\Delta\varphi_m = \frac{2\pi L_{sw}(n_r - n_m)}{\lambda_0} \quad (1)$$

Where:

- λ_0 = wavelength of the light used
- L_{sw} = sensing window length (related to the effective distance where the light propagates and interacts)
- n_r = effective index of the reference arm
- n_m = effective index of the measurement arm

Therefore, in equation (1), there is a linear change in the phase shift due to the variation in the refractive index. The MZWI output is a function of the phase shift; when the output reaches the maximum point, the phase shift is zero ($\Delta\varphi_m = 0$), and when the output achieves the minimum point, the phase shift is $\Delta\varphi_m = \pi$ (Schubert *et al.*, 1997).

The BeamPROP™ simulation tool (RSoft Photonics CAD suite) was used to simulate the MZWI. The following parameters were used to design the MZWI structure: wavelength $\lambda = 642$ nm, refractive index $n = 1.4577$, change in the refractive index $\Delta n = 0.0013$ (Nolte *et al.*, 2003) (corresponding to previous works on fused silica), and component height = component width = $15 \mu\text{m}$ (this value was set to make the simulation as real as possible, corresponding to work previously performed in the laboratory). In addition, the total length of the MZWI was $8000 \mu\text{m}$, the separation between the reference and measurement branches was $170 \mu\text{m}$, and the radius of the s-bend arcs was $41491.9 \mu\text{m}$. A large radius of curvature on the order of millimeters or hundreds of microns was necessary due to the modal behavior, in which the mode is pulled outwards as the waveguide changes direction, forming a distorted mode (see Figure 1) (Zappe, 1994). Similarly, the length

of the sensing window was set to $55 \mu\text{m}$ because the microchannel in which it is integrated has a width of $50 \mu\text{m}$ with a tolerance of $\pm 2.5 \mu\text{m}$.

1 × 4 OPS

The OPS configuration is one of the most common applications of photonic devices and is usually formed with a back-to-back waveguide bend geometry with a symmetrical structure based on a sinusoidal shape function for the analysis of the s-shaped bend. Figure 1 shows the geometry of a sinusoidal curve of length L that links two parallel guides when displaced by a transversal distance l .

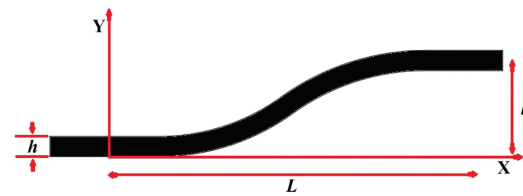


Figure 1. S-shaped waveguide bend geometry

Based on this structure, the simulation of the 1×4 OPS was performed using the BeamPROP™ tool, with the same parameters as those used for the MZWI: wavelength $\lambda = 642$ nm, refractive index $n = 1.4577$, change in refractive index $\Delta n = 0.0013$, component height = component width = $15 \mu\text{m}$, total length = $8000 \mu\text{m}$, separation between waveguides W1, W2, W3, and W4 = $250 \mu\text{m}$, and sensing window length = $55 \mu\text{m}$.

DESIGN IN AUTOCAD®

To obtain the designs of the photonic devices, the DXF files of the structures were exported to AutoCAD® software, where the necessary parameters and final coordinates to complete their manufacture in the micro-machining station were set. A schematic representation of the proposed integrated photonic devices is shown in Figure 2.

FABRICATION

MANUFACTURE OF PHOTONIC DEVICES IN FUSED SILICA

A MZWI and a 1×4 OPS were fabricated in commercial fused silica glass (Corning 7980) with dimensions of $8 \text{ mm} \times 8 \text{ mm} \times 1.1 \text{ mm}$ and a refractive index n of 1.4577 . The process was carried out with Newport $\mu\text{FAB}^{\text{TM}}$ micromachining station software ($\mu\text{FAB} 3.9.13$) and an ultrafast Libra Coherent femtosecond laser with a central wavelength of 800 nm , a repetition rate of 1 kHz , a pul-

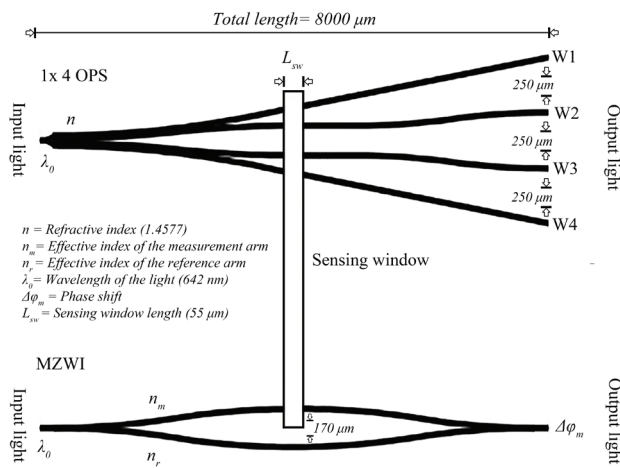


Figure 2. Schematic representation of the integrated photonic devices

se duration of 50 fs, an average power of 3.8 W, total distances in the XYZ axes of 100 mm × 100 mm × 5 mm, a resolution of 0.05 μm and a speed on the XY axes of 300 mm/s. The femtosecond laser system has an amplification that exceeds the power needed for the fabrication of optical waveguides and microchannels in this material; thus, by using a rotating half-wave plate (HWP) and a static polarizer (P), variable attenuation of the emitted laser light is possible. As a result, the incident laser beam of the laser source can be controlled by the μFAB™ station software through a PC, which attenuates the power with the HWP and P; in addition to performing the analog-to-digital conversion of the signals for controlling the movements of the XYZ micro-positioner. The system was also equipped with a charge-coupled device (CCD) camera to observe the micromachining process. Figure 3 shows a schematic representation of the system used for writing waveguides to form microstructures using a femtosecond laser.

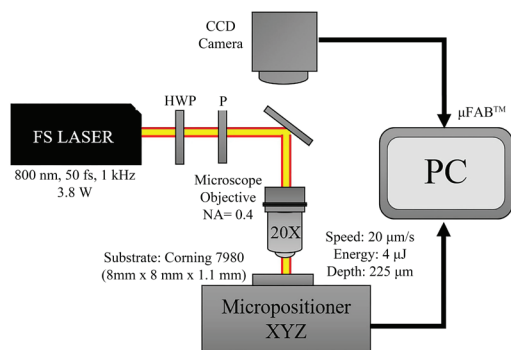


Figure 3. Schematic representation of the experimental setup for femtosecond laser writing

The manufacturing parameters were established based on the literature for this material, including the translation speed (20 μm/s), energy (4 μJ), and depth (225 μm), and its production was achieved using a microscope objective with numerical aperture NA = 0.4. The effects of translation speed and laser power on the process were evaluated to identify the ideal parameters for the fabrication of photonic devices. For the MZWI, a separation of 170 μm between the branches was defined to achieve lower radiation losses because larger separations increase the radiation losses in the device. Based on the simulation results, the writing of the photonic devices was performed using a femtosecond laser with an ideal pulse energy of 4 μJ. For lower energy values, the quality of the waveguides began to decrease, and for higher energy values, the substrate became damaged. In addition, the ideal writing speed was found to be 20 μm/s based on the design of the s-bend waveguides because speeds lower than 50 μm/s kept the light inside the structure perfectly confined. For higher speeds, there was a greater decrease in the amount of light at the exit.

INTEGRATION OF THE MICROFLUIDIC CHANNEL WITH THE PHOTONIC DEVICES

The 3D design of the microfluidic channel was based on the SC-FLICE technique using conical spirals according to the literature by means of equation (2) (Vishnubhatla *et al.*, 2009):

$$\alpha_{ang} = \tan^{-1} \left(\frac{r_s}{L_s} \right) \quad (2)$$

Where:

L_s = length of the channel

r_s = radius of the channel

α_{ang} = resulting angle

The values for L_s and r_s were 750 μm and 25 μm (circular cross-section), respectively. Since α_{ang} must have a constant value of 1.9° to achieve inverse engraving during the chemical treatment, longer microchannels with a uniform cross-section were obtained by varying the length of the cone that was irradiated and, as a result, the engraving time.

The energy doses and translation speed were varied at key points during production by the micromachining station software, defining sections for each segment irradiated by the femtosecond laser, thus facilitating the writing process and introducing continuity at the link of each part.

In addition, based on the periodicity Λ of the spirals, the degree of superposition between two successive laser irradiated arcs in the conical spiral can be determined. Because there is insufficient overlap, the acid encounters unexposed regions, causing the engraving process to slow down; thus, $\Lambda = 2 \mu\text{m}$ is the ideal value based on the literature (Vishnubhatla *et al.*, 2009). Therefore, the 3D design consisted of a microfluidic channel with a total length of 6 mm and two helices with radii of $100 \mu\text{m}$ as access holes at a depth of $200 \mu\text{m}$. The structure of the microfluidic channel was formed with two helices with lengths of $410 \mu\text{m}$ and radii of $2.5 \mu\text{m}$ starting at each edge, followed by conical spirals with lengths of $750 \mu\text{m}$ and radii of $25 \mu\text{m}$ at each edge of the microfluidic channel. In the central part, there were six additional helices with lengths of $750 \mu\text{m}$, $400 \mu\text{m}$, and $450 \mu\text{m}$ with radii of $25 \mu\text{m}$. Finally, a straight line was used as the central axis of each structure, all of which were joined at their ends. Once the 3D design was completed, the microfluidic channel was fabricated by selecting appropriate manufacturing parameters, such as the translation speed, energy dose, and depth ($225 \mu\text{m}$). The impact of translation speed was determined based on the results obtained from various experiments using speeds ranging from 20 to $200 \mu\text{m/s}$ with a constant pulse energy of $4 \mu\text{J}$. Based on the average translation speed of $20 \mu\text{m/s}$ reported in similar studies (Maselli *et al.*, 2006; Vishnubhatla *et al.*, 2009), more homogeneous patterns were formed because there was a greater amount of energy deposited per unit volume, increasing the engraving speed through chemical attack. However, this effect decreases as the translation speed increases. As a result, for the access holes (helices), a pulse energy of $2 \mu\text{J}$ was established at a speed of $50 \mu\text{m/s}$ because the access holes were arrays with larger diameters. For the conical spirals, an energy of $3 \mu\text{J}$ was established at a speed of $100 \mu\text{m/s}$ since the spirals are structures with regular diameters and a longer length. For the central lines of each structure, an energy of $4 \mu\text{J}$ was established at a speed of $20 \mu\text{m/s}$ since the central lines are the basis of each structure. As a result, the microfluidic channel and photonic devices were written by the system software with the coordinates obtained in AutoCAD® (Figure 4), changing only the manufacturing values corresponding to each system part to enable a higher degree of precision during the manufacturing process. The photonic devices were strategically placed approximately in the middle of the microfluidic channel, where the dimensions were smaller, to achieve greater precision in the data during characterization (MZWI and OPS were perpendicular to the microfluidic channel). Subsequently, chemical treatment was carried out using the SC-FLICE techni-

que, which was realized by placing the substrate in an aqueous solution of commercial hydrofluoric acid (Jalmek, with 48-51 % purity) in vials at 20 % concentration with a degree of acidity (pH) of 2.99 using an ultrasonic bath (Cole-Parmer 8893) with an output frequency of 40 kHz for approximately 6.5 hours at a temperature of 40°C .

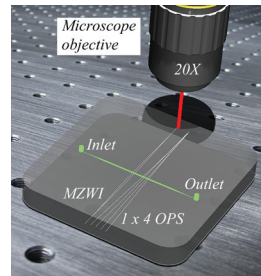


Figure 4. Schematic of the laser-written structures

CHARACTERIZATION OF THE SYSTEM

PHOTONIC DEVICES

The waveguides that make up the photonic devices were characterized with an experimental setup based on an XYZ micropositioning system (Newport 561D) and a multichannel-coupled fiber laser source system (Thorlabs MCLS1) that coupled the 642 nm light with a typical power of 20 mW inside the photonic devices and the guided light via a microscope objective with a magnification of 20X at the exit of the waveguide. Thus, to obtain the propagation loss coefficient (α), equation (3) was used in accordance with the literature (Bourhis, 1994):

$$\alpha = -\frac{10}{L_g} \log_{10} \frac{T_g}{\eta_{ac} T_F} \quad (3)$$

Where:

L_g = length of the waveguide

T_g = transmittance of the waveguide

T_F = Fresnel transmission coefficient at the output of the waveguide

η_{ac} = coefficient of coupling losses

Figure 5 shows the experimental setup for measuring the input and output powers of each waveguide using a Thorlabs PM100D power meter and the waveguide mode dimensions with a Thorlabs BC106-VIS CCD camera.

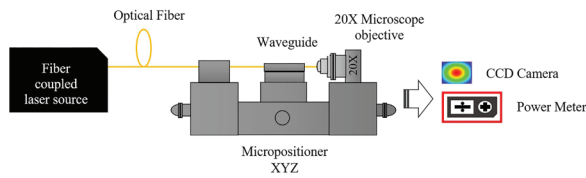


Figure 5. Schematic representation of the experimental setup used to measure the power, laser beam waist, and mode dimensions in the waveguides

The change in the refractive index (Δn) can be calculated based on the numerical aperture of the waveguides, where the guided light is projected directly onto a screen located at distance d from the output face of the waveguide, removing the 20X microscope objective (Figure 6). An interference pattern in the form of rings can be seen in the far field, and the radius r where the fringes vanished was measured for different values of d , yielding five measurements that were averaged to calculate the r/d ratio in each of the waveguides. It was observed that the distance d varied linearly with the fringe radius, which means that the r/d ratio has a constant linear slope. Thus, the numerical aperture of the waveguides can be estimated by the average value of r/d (Dharmadhikari *et al.*, 2011):

$$NA = \sin\left(\arctan\left(\frac{r}{d}\right)\right) \quad (4)$$

Given that:

$$NA = \sqrt{2n\Delta n} \quad (5)$$

Where n is the refractive index of the bulk material and NA is the numerical aperture, as shown in equation (4) and equation (5), the change in the refractive index (Δn) can be obtained.

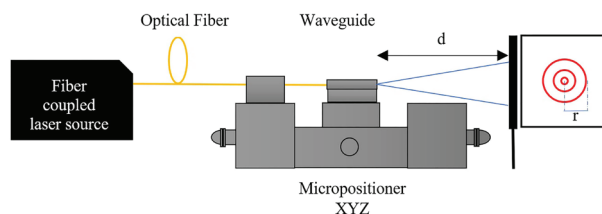


Figure 6. NA calculation based on r/d

MICROFLUIDIC CHANNEL

Using a VHX-5000 digital microscope at 500X magnification with autofocus, cross-sectional views of the microchannel were obtained by measuring its dimensions before chemical treatment to verify that the writing

with the femtosecond laser was correct. Figure 7 shows the diameter measurement ($50 \mu\text{m}$) of one of the microchannel sections with a length of $750 \mu\text{m}$.

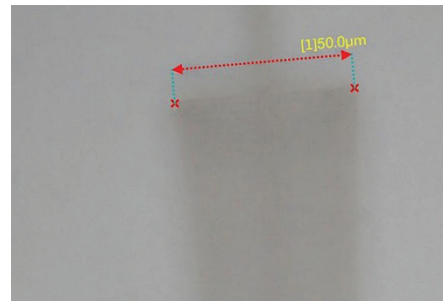


Figure 7. Microchannel image before chemical treatment

RESULTS AND DISCUSSION

PHOTONIC DEVICES

The MZWI was simulated using the beam propagation method (BPM) to determine the feasibility of the proposed structure based on s-bend waveguides, with an analysis of both branches. Based on the obtained results, a separation of $55 \mu\text{m}$ (sensing window) in one of its branches was capable of confining the light and achieving a sensing signal at the exit of the junction of both branches. A refractive index $n = 1.4577$ was directly acquired from the measurement of the fused silica substrate by means of the prism coupling method in a Metricon 2010M, achieving results that are similar to real-world measurements at the time of manufacture. The change in the refractive index in the MZWI ($\Delta n = 1.3 \times 10^{-3}$) was defined based on previous reports, and, together with the optical path length, the phase changes of the light were obtained when the beam was coupled through the sensing window (monitoring a range of $0 - 200 \mu\text{m}$), while the reference branch was kept constant, allowing the calculation of the optical transmission through repeated iterations to visualize the phase difference of the device in both branches. Some of the real factors that could affect the simulation could be inhomogeneities, which can reduce the quality of the interferometer and increase losses; aberrations generated when focusing the beam during the manufacturing process, the beam would then not be truly circular; and the refractive index profile, since a step index was assumed and there could have been some variations in the real profile although the impact would be minimal in this case since the profile is approximately step. Figure 8 shows the level of transmission achieved by the MZWI when the light crossed the entire device with a $55 \mu\text{m}$ sensing window, and a transmission percentage of 54.79% was shown to obtain the work point of the

device. Thus, the light confined through the device guarantees an adequate power output at the output branches.

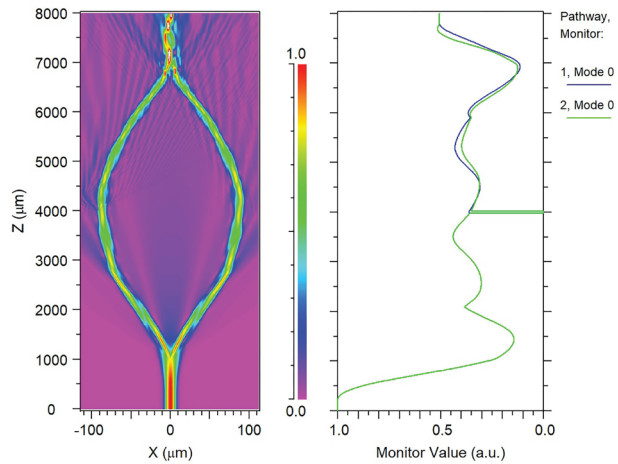


Figure 8. Simulation of the MZWI with s-bend waveguides with transmission of 54.79 %

Similarly, a simulation of the OPS was performed using the BPM method to verify the proposed design with the same parameters as those used in the previous simulation for the MZWI, such as the waveguide width and refractive index, since both devices were manufactured using the same writing process. When light was introduced at the input of the OPS, it began to propagate through the structure and was divided into four approximately equal parts with small variations in the transmission of the waveguides that lie on the edges (W1, W4) with respect to the central channels. Figure 9 shows the four channels corresponding to waveguides W1, W2, W3, and W4. The fundamental mode was simulated to analyze the optical paths from the beginning of the photonic device, through the sensing window, and finally to the end of each waveguide. Hence, an area defined by a sensing window of 55 μm allows the variation in transmission that the light experiences when passing through the window to be observed, indicating that the light remains sufficiently confined, as reported in previous works (Martinez-Vazquez *et al.*, 2009).

Figure 10 shows the percentage of transmission as a function of the sensing window length, which was 18.46 % for waveguides W1 and W4, and 21.41 % for waveguides W2 and W3 for a sensing window length of 55 μm. The lower transmission of waveguides W1 and W4 is due to their greater curvature. The longer the separation between the channels, the more the transmission tends to reduce as the curves become more pronounced. Consequently, the existence of light leaks causes transmission losses in the device as the separation increases.

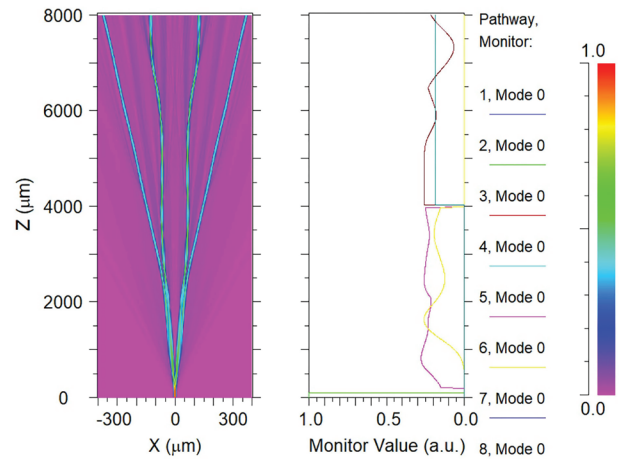


Figure 9. Simulation of the 1 × 4 OPS

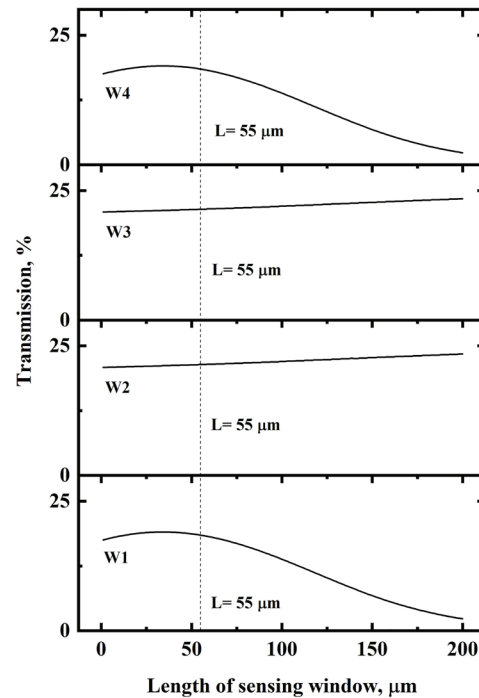


Figure 10. Output transmission as a function of the sensing window length for the 1 × 4 OPS

The near-field distribution intensity profiles of the photonic devices are shown in Figure 11a and Figure 12a, b, c, and d; in Figure 11b and Figure 12e, the propagation modes obtained by BeamPROP™ are shown. The fundamental mode was confined in all the devices, and the shadows seen on the sides of the mode in Figure 11b could be attributed to the light that escaped from the curved channels and junctions. Figures 11c and 12f depict the refractive index profiles for the MZWI and the 1 × 4 OPS, respectively, on a 50:1 scale, with optimized dimensions of a total length of 8000 μm, a light wavelength of 642 nm, and a refractive index change

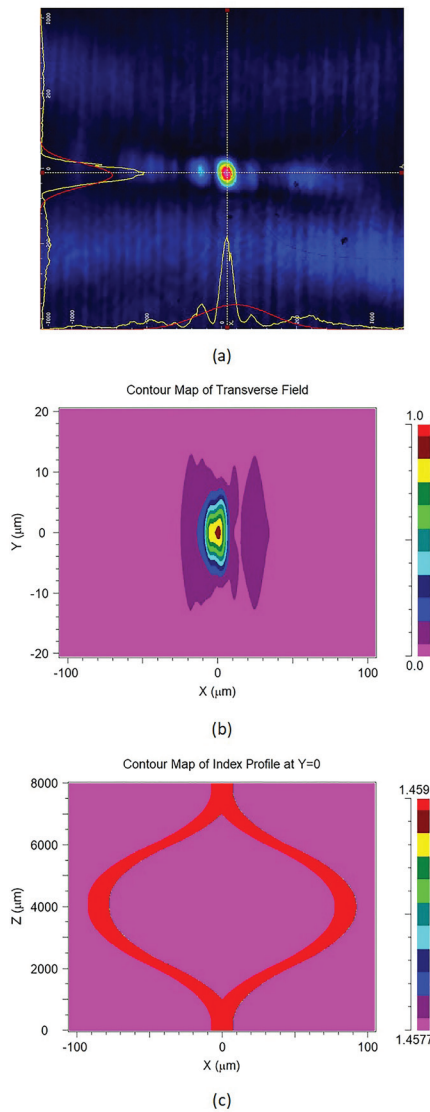


Figure 11. a) Near-field distribution intensity profile of the MZWI, b) propagation mode obtained by BeamPROP™ for the MZWI, c) refractive index profile for the MZWI

$\Delta n = 0.0013$. There was a similarity between the propagation modes observed in the modeling of RSoft and those observed after the devices were manufactured by laser writing.

The photonic devices were written at a depth of 225 μm below the surface, perpendicular to the cross-section of the microfluidic channel (located 2.5 μm from the wall of the microchannel on both sides, avoiding possible damage during its manufacture). The waveguides had an average width/thickness of 5 - 15 μm ; the width/thickness of the MZWI were 6.45 μm / 8.12 μm , respectively, and the widths/thicknesses for the OPS were: W1 (7.1 μm / 14.2 μm), W2 (5.16 μm / 14.2 μm), W3 (4.84 μm / 13.85 μm) and W4 (5.16 μm / 13.25 μm).

The refractive index increase calculated using the far-field method was 4.47×10^{-4} for the MZWI and 3.46×10^{-4} for the OPS, with an error of $\sim 30\%$. It has been reported that the absorption of laser energy by the sample, as well as the dissipation of the energy absorbed within the irradiated material, can be possible causes of refractive index modification and subsequent waveguide formation (Gattass *et al.*, 2008). The propagation losses of the 1×4 OPS were found to be 11.2 dB/cm, 9.99 dB/cm, 9.79 dB/cm and 10.69 dB/cm for waveguides W1, W2, W3 and W4, respectively. These results are similar to those obtained in (Yuan *et al.*, 2015), where the losses were mainly attributed to energy dissipation at the junction point of the waveguides. On the other hand, the propagation losses for the MZWI were 13.45 dB/cm, which may be due to the greater angle at the junctions, the curvature of the branches and the length of the structure.

MICROFLUIDIC CHANNEL

Remarkable uniformity was obtained in the microfluidic channel structure when the conical shapes were compensated using the SC-FLICE technique. Diameters

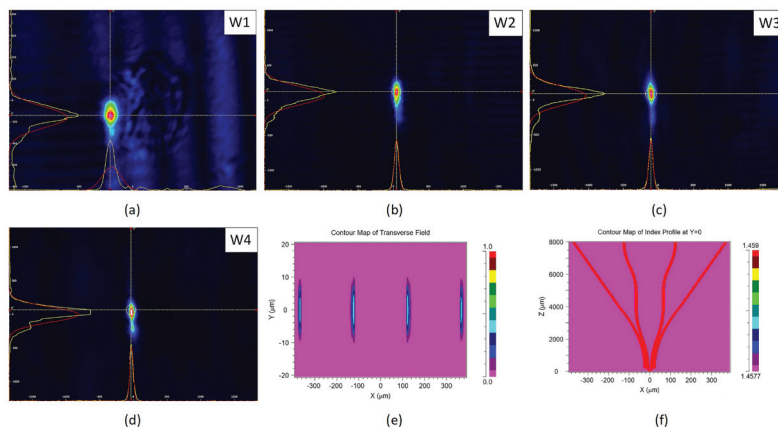


Figure 12. a), b), c), d) Near-field distribution intensity profile for each of the waveguides of the 1×4 OPS, e) propagation modes obtained by BeamPROP™ for the 1×4 OPS, f) refractive index profile for the 1×4 OPS

of 475.5 μm were obtained for the access holes and a width of 54.15 μm was obtained for the microfluidic channel, as shown in Figure 13a. A microfluidic channel with a more uniform cylindrical shape was observed, and the expected parameters were obtained after the manufacturing process with photonic devices outside the microfluidic channel, which allowed adequate light confinement. This was because the SC-FLICE technique was used; in contrast, the FLICE technique would form uncompensated conical geometries, which would not favor the design, as they would deform when attempting to reach the buried regions without being able to penetrate the regions. In addition, this technique requires a longer engraving time and destroys the entire substrate by exposing the microfluidic channel. However, the access holes were deformed, which can be attributed to the longer manufacturing time and use of a greater amount of HF, as shown in Figure 13b. A possible solution to avoid damage to the substrate due to HF could be coating the material before chemical attack at the same manufacturing site with an asphalt paint mask, commonly known as the bitumen of Judea, which avoids the destruction of the substrate by increasing its resistance to HF, obtaining a high-quality microfluidic channel, and then applying a second laser marking on the access holes to release the input to the microchannel. In this context, this work demonstrates that it is possible to create longer microfluidic channels, as well as photonic devices integrated in a single chip, for use as biosensors (Figure 13c).

CONCLUSIONS

In conclusion, photonic devices and a uniform microfluidic channel were obtained by using ultrafast laser writing. The photonic devices had waveguides with widths and thicknesses ranging from 5 to 15 μm and a total length of 8000 μm . α values of 13.45 dB/cm were achieved for the MZWI, and α values of 11.2 dB/cm, 9.99 dB/cm, 9.79 dB/cm and 10.69 dB/cm were achieved for the OPS. The changes in the refractive index (Δn) for the OPS and the MZWI were 4.47×10^{-4} and 3.46×10^{-4} , respectively, which is on the order of the proposed $\Delta n = 1.3 \times 10^{-3}$ in the simulation. In addition, it was demonstrated that with the application of the SC-FLICE technique, ideal parameters are required to obtain uniformity and a longer microfluidic channel length. A microfluidic channel with a diameter of 54.15 μm and length of 6000 μm was obtained. Thus, due to the long immersion time in HF acid, the access holes were deformed. However, in the next work, a protective mask could be used to prevent the inlet holes from deforming and to improve their quality. Thus, the integration of

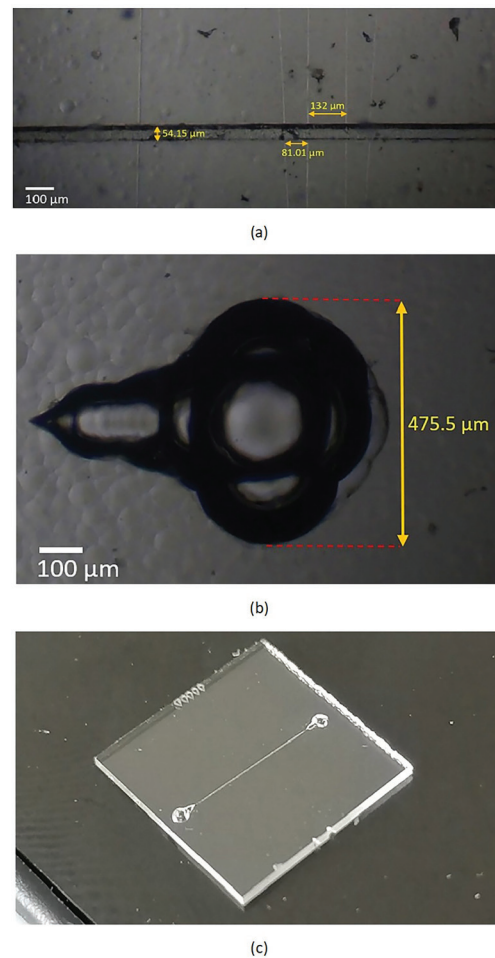


Figure 13. a) Uniformity in the microfluidic channel, b) deformation of access holes, c) microfluidic channel and photonic devices integrated in a single chip

photonic devices with microfluidic channels has significant potential. The results show that an optofluidic system can be developed to detect biological and chemical substances introduced into the microfluidic channel with photonic devices that can be used for real-time monitoring and diagnosis. In future work, a multisensory system that uses microfluidic channels and waveguides in conjunction with integrated electronic devices, such as microcontrollers, will be developed to expand the sensor detection field and decrease propagation losses by varying the radius of curvature to reduce the light lost by radiation.

ACKNOWLEDGEMENTS

Jiménez-Ávila Daniel thanks Dr. Jiménez-Islas Hugo for his assistance in publishing this research paper. **Funding.** CONAHCYT (Scholarship #401177 and grant CF-376135).

REFERENCES

- Asrar, P., Sucur, M., & Hashemi, N. (2015). Multi-pixel photon counters for optofluidic characterization of particles and microalgae. *Biosens.*, 5, 308-318. <https://doi.org/10.3390/bios5020308>
- Bellini, N., Bragheri, F., Cristiani, I., Guck, J., Osellame, R., & Whyte, G. (2012). Validation and perspectives of a femtosecond laser fabricated monolithic optical stretcher. *Biomed. Opt. Express*, 3, 2658. <https://doi.org/10.1364/boe.3.002658>
- Bing, P., Yao, J., Lu, Y., & Li, Z. (2012). A surface-plasmon-resonance sensor based on photonic-crystal-fiber with large size microfluidic channels. *Opt. Appl.*, 42, 493-501. <https://doi.org/10.5277/oa120306>
- Bourhis, J.-F. (1994). Fiber-to-waveguide connection. *Glas. Integr. Opt. Opt. Fiber Devices A Crit. Rev.*, 10275, 102750L. <https://doi.org/10.1117/12.179761>
- Chandrahali, H., Chen, Q., Said, A. A., Dugan, M., & Fan, X. (2015). Monolithic optofluidic ring resonator lasers created by femtosecond laser nanofabrication. *Lab Chip*, 15, 2335-2340. <https://doi.org/10.1117/12.17976110.1039/c5lc00254k>
- Devayani, I. J., Syahriar, A., & Astharini, D. (2014). Characteristics of S-bend optical waveguides based on back-to-back and sinusoidal structures. Proc. 2014 International Conference on Electrical Engineering and Computer Science, ICEECS 2014, 2, 65-68. <https://doi.org/10.1109/ICEECS.2014.7045221>
- Dharmadhikari, J. A., Dharmadhikari, A., Bhatnagar, A., Mallik, A., Chandrakanta Singh, P., Dhaman, R. K., . . . Mathur, D. (2011). Writing low-loss waveguides in borosilicate (BK7) glass with a low-repetition-rate femtosecond laser. *Opt. Commun.*, 284, 630-634. <https://doi.org/10.1016/j.optcom.2010.09.055>
- Gao, R., Lu, D. F., Cheng, J., Jiang, Y., Jiang, L., Xu, J. D., & Qi, Z. M. (2016). Fiber optofluidic biosensor for the label-free detection of DNA hybridization and methylation based on an inline tunable mode coupler. *Biosens. Bioelectron.*, 86, 321-329. <https://doi.org/10.1016/j.bios.2016.06.060>
- Gattass, R. R., & Mazur, E. (2008). Femtosecond laser micromachining in transparent materials. *Nat. Photonics*, 2, 219-225. <https://doi.org/10.1038/nphoton.2008.47>
- Haque, M., Lee, K. K., Ho, S., Fernandes, L. A., & Herman, P. R. (2014). Chemical-assisted femtosecond laser writing of lab-in-fibers. *Lab Chip*, 14, 3817-3829. <https://doi.org/10.1039/c4lc00648h>
- Heideman, R., & Lambeck, P. (1999). Remote opto-chemical sensing with extreme sensitivity: Design, fabrication and performance of a pigtailed integrated optical phase-modulated Mach-Zehnder interferometer system. *Sensors Actuators, B Chem.*, 61, 100-127. [https://doi.org/10.1016/S0925-4005\(99\)00283-X](https://doi.org/10.1016/S0925-4005(99)00283-X)
- Kee, J. S., Poenar, D. P., Neuzil, P., & Yobas, L. (2008). Monolithic integration of poly (dimethylsiloxane) waveguides and microfluidics for on-chip absorbance measurements. *Sensors Actuators, B Chem.*, 134, 532-538. <https://doi.org/10.1016/j.snb.2008.05.040>
- Krol, D. M. (2008). Femtosecond laser modification of glass. *J. Non. Cryst. Solids*, 354, 416-424. <https://doi.org/10.1016/j.jnoncrysol.2007.01.098>
- Leistiko, O., & Jensen, P. F. (1998). Integrated bio/chemical microsystems employing optical detection: The clip-on. *J. Micro-mechanics Microengineering*, 8, 148-150. <https://doi.org/10.1088/0960-1317/8/2/026>
- Li, Z., Xu, Y., Fang, W., Tong, L., & Zhang, L. (2015). Ultra-sensitive nanofiber fluorescence detection in a microfluidic chip. *Sensors (Switzerland)*, 15, 4890-4898. <https://doi.org/10.3390/s150304890>
- Liu, C., Xiao, T., Wang, Y., Wang, F., & Chen, X. (2017b). Rhodamine based turn-on fluorescent sensor for Hg²⁺ and its application of microfluidic system and bioimaging. *Tetrahedron*, 73, 5189-5193. <https://doi.org/10.1016/j.tet.2017.07.012>
- Liu, K., Yang, Q., Zhao, Y., Chen, F., Shan, C., He, S., . . . Bian, H. (2014). Three-dimensional metallic microcomponents achieved in fused silica by a femtosecond-laser-based microsolidifying process. *Microelectron. Eng.*, 113, 93-97. <https://doi.org/10.1016/j.mee.2013.07.017>
- Liu, L., Zhou, X., Wilkinson, J. S., Hua, P., Song, B., & Shi, H. (2017a). Integrated optical waveguide-based fluorescent immunosensor for fast and sensitive detection of microcystin-LR in lakes: Optimization and Analysis. *Sci. Rep.*, 7, 1-9. <https://doi.org/10.1038/s41598-017-03939-8>
- Luchansky, M. S., & Bailey, R. C. (2012). High-Q optical sensors for chemical and biological analysis. *Anal. Chem.*, 84, 793-821. <https://doi.org/10.1021/ac2029024>
- Martinez-Vazquez, R., Nava, G., Vegliione, M., Yang, T., Bragheri, F., Minzioni, P., . . . Cristiani, I. (2015). An optofluidic constriction chip for monitoring metastatic potential and drug response of cancer cells. *Integr. Biol. (United Kingdom)*, 7, 477-484. <https://doi.org/10.1039/c5ib00023h>
- Martinez-Vazquez, R., Osellame, R., Nolli, D., Dongre, C., Van Den Vlekkert, H., Ramponi, R., . . . Cerullo, G. (2009). Integration of femtosecond laser written optical waveguides in a lab-on-chip. *Lab Chip*, 9, 91-96. <https://doi.org/10.1039/b808360f>
- Maselli, V., Osellame, R., Cerullo, G., Ramponi, R., Laporta, P., Magagnin, L., & Cavallotti, P. L. (2006). Fabrication of long microchannels with circular cross section using astigmatically shaped femtosecond laser pulses and chemical etching. *Appl. Phys. Lett.*, 88, 191107. <https://doi.org/10.1063/1.2203335>
- Nolte, S., Will, M., Burghoff, J., & Tuennermann, A. (2003). Femtosecond waveguide writing: A new avenue to three-dimensional integrated optics. *Appl. Phys. A Mater. Sci. Process*, 77, 109-111. <https://doi.org/10.1007/s00339-003-2088-6>
- Olyaei, S., Seifouri, M., Sourani, E. A., & Dhasarathan, V. (2020). Design and numerical analysis of an all-optical 4-channel power splitter in E, S, C, L, and U bands via nano-line defects in photonic crystal. *J. Opt. Commun.*, 41, 241-247. <https://doi.org/10.1515/joc-2017-0194>
- Osellame, R., Hoekstra, H. J., Cerullo, G., & Pollnau, M. (2011). Femtosecond laser microstructuring: An enabling tool for op-

- tofluidic lab-on-chips. *Laser Photonics Rev.*, 5, 442-463. <https://doi.org/10.1002/lpor.201000031>
- Païè, P., Bragheri, F., Bassi, A., & Osellame, R. (2016). Selective plane illumination microscopy on a chip. *Lab Chip*, 16, 1556-1560. <https://doi.org/10.1039/c6lc00084c>
- Païè, P., Bragheri, F., Martínez Vázquez, R., & Osellame, R. (2014). Straightforward 3D hydrodynamic focusing in femtosecond laser fabricated microfluidic channels. *Lab Chip*, 14, 1826-1833. <https://doi.org/10.1039/c4lc00133h>
- Patel, P. B., & Hamde, S. T. (2017). Analysis of the Mach-Zehnder interferometer waveguide structure for refractive index measurement. *J. Opt.*, 46, 398-402. <https://doi.org/10.1007/s12596-017-0391-4>
- Pham, S. V., Dijkstra, M., Hollink, A. J., Kauppinen, L. J., De Ridder, R. M., Pollnau, M., . . . Hoekstra, H. J. (2012). On-chip bulk-index concentration and direct, label-free protein sensing utilizing an optical grating-waveguide cavity. *Sensors Actuators, B Chem.*, 174, 602-608. <https://doi.org/10.1016/j.snb.2012.08.002>
- Rajesh, S., & Bellouard, Y. (2010). Towards fast femtosecond laser micromachining of fused silica: The effect of deposited energy. *Opt. Express*, 18, 21490. <https://doi.org/10.1364/oe.18.021490>
- Schubert, T., Haase, N., & Ktück, H. (1997). Refractive-index measurements using an integrated Mach-Zehnder interferometer. *Sensors Actuators, A Phys.*, 60, 108-112. [https://doi.org/10.1016/S0924-4247\(97\)01380-0](https://doi.org/10.1016/S0924-4247(97)01380-0)
- Vishnubhatla, K. C., Bellini, N., Ramponi, R., Cerullo, G., & Osellame, R. (2009). Shape control of microchannels fabricated in fused silica by femtosecond laser irradiation and chemical etching. *Opt. Express*, 17, 8685. <https://doi.org/10.1364/oe.17.008685>
- Xia, J., Rossi, A. M., & Murphy, T. E. (2012). Laser-written nanoporous silicon ridge waveguide for highly sensitive optical sensors. *Opt. Lett.*, 37, 256. <https://doi.org/10.1364/ol.37.000256>
- Yadav, T. K., Narayanaswamy, R., Bakar, M. H., Kamil, Y. M., & Mahdi, M. A. (2014). Single mode tapered fiber-optic interferometer based refractive index sensor and its application to protein sensing. *Opt. Express*, 22, 22802. <https://doi.org/10.1364/oe.22.022802>
- Yuan, W.-H., Lv, J.-M., Hao, X.-T., & Chen, F. (2015). Optimization of waveguide structures for beam splitters fabricated in fused silica by direct femtosecond-laser inscription. *Opt. Laser Technol.*, 74, 60-64. <https://doi.org/10.1016/j.optlastec.2015.05.016>
- Zappe, H. P. (1994). Introduction to semiconductor optics. *Choice Rev. Online*, 31, 31-5515. <https://doi.org/10.5860/choice.31-5515>
- Zhao, M., Hu, J., Jiang, L., Zhang, K., Liu, P., & Lu, Y. (2015). Controllable high-throughput high-quality femtosecond laser-enhanced chemical etching by temporal pulse shaping based on electron density control. *Sci. Rep.*, 5, 1-9. <https://doi.org/10.1038/srep13202>

Cómo citar:

Jiménez-Ávila, D., Vázquez, G. V., & Soto-Bernal, J. J. (2025). Design and fabrication of photonic devices and a microfluidic channel with a femtosecond laser. *Ingeniería Investigación y Tecnología*, 26(01), 1-11. <https://doi.org/10.22201/fi.25940732e.2025.26.1.007>